



This is a repository copy of *Engineering the locusts: Hind leg modelling towards the design of a bio-inspired space hopper*.

White Rose Research Online URL for this paper:
<http://eprints.whiterose.ac.uk/96344/>

Version: Accepted Version

Article:

Punzo, G. and McGookin, E.W. (2016) Engineering the locusts: Hind leg modelling towards the design of a bio-inspired space hopper. Proceedings of the Institution of Mechanical Engineers, Part K: Journal of Multi-body Dynamics. 1464419315624852. ISSN 1464-4193

<https://doi.org/10.1177/1464419315624852>

Reuse

Unless indicated otherwise, fulltext items are protected by copyright with all rights reserved. The copyright exception in section 29 of the Copyright, Designs and Patents Act 1988 allows the making of a single copy solely for the purpose of non-commercial research or private study within the limits of fair dealing. The publisher or other rights-holder may allow further reproduction and re-use of this version - refer to the White Rose Research Online record for this item. Where records identify the publisher as the copyright holder, users can verify any specific terms of use on the publisher's website.

Takedown

If you consider content in White Rose Research Online to be in breach of UK law, please notify us by emailing eprints@whiterose.ac.uk including the URL of the record and the reason for the withdrawal request.



eprints@whiterose.ac.uk
<https://eprints.whiterose.ac.uk/>

Engineering the Locusts. Hind Leg Modelling
Towards the Design of a Bio-Inspired Space
Hopper

Giuliano Punzo^{1,2} and Euan W. McGookin¹

¹Division of Aerospace Sciences, School of Engineering, University
of Glasgow, UK

²Department of Mechanical and Aerospace Engineering, University
of Strathclyde, Glasgow

March 11, 2016

Abstract

The mechanical operation of a biologically inspired robot hopper is presented. This design is based on the hind leg dynamics and jumping gait of a desert locust (*schistocerca gregaria*). The biological mechanism is represented as a lumped mass system. This emulates the muscle activation sequence and gait responsible for the long, coordinated jump of locusts, whilst providing an engineering equivalent for the design of a biological inspired hopper for planetary exploration.

Despite the crude simplification, performance compares well against biological data found in the literature and scaling towards size more typical of robotic realisation are considered from an engineering point of view. This

aspect makes an important contribution to knowledge as it quantifies the balance between biological similarity and efficiency of the biomimetic hopping mechanism. Further, this work provides useful information towards the biomimetic design of a hopper vehicle whilst the analysis uncover the range maximisation conditions for powered flight at constant thrust by analytic means. The proposed design bridges concepts looking at the gait dynamics and designs oriented to extended, full powered trajectories.

Keywords

Hopper, Hind Leg Modelling, Biomimetic, Space Exploration, Design Study, Locust

1 Introduction

Beside being extremely interesting from the biological point of view, grasshoppers and locusts can provide inspiration for engineering design. The ability to perform long jumps, with a wing-aided aerial stage [1], makes them a model for a particular hybrid engineering vehicle known as “*hopper*”. As different from wheeled robots, hoppers can overcome obstacles bigger than their size by jumping over them: this characteristic makes them extremely useful for traversing rocky and steep terrains, often found in the context of planetary exploration [2–4].

Popular designs foresee either pure hopping dynamics, or dynamics with an extended aerial motion enhanced by the application of thrust. In the first case the hopper relies on the propulsive forces produced by the leg mechanisms (see the examples in [5–7]). In the second, a flying stage is aided by rockets or other means e.g. glider wings. In both cases the legs are used in the final stage to land and possibly regain energy. An example can be found in [8]. The two concepts are substantially different. Hoppers that are propelled by legs only are

conceived in a framework of repeated, short jumps, with the attention focussed on the gait dynamics. In contrast, hoppers making use of other forms of propulsion in addition to legs perform short powered flights rather than jumps. They cover long distances and use the legs as support devices when on the ground. Some examples of the two concepts can be found in the literature. Brown and Zeglin [9], for example, proposed a simple bow mechanism storing energy by bending through the aerial stage and releasing it at touchdown. This minimalist design appears to be more applicable for small vehicles and relatively short, frequent jumps.

In [10], the authors present a design for a jumping robot with two actuators providing impulsive torques at the joints. This design does not consider flexible elements. It focusses on actuators delivering impulsive torque at the joints so that a gait, rather than a jump, is completed. The authors validate this design through experiments and analyse the dynamics mainly through numerical means with the motion broken down in four main phases.

In contrast, Fiorini *et al.* [5] present a hopper design based on pure hopping dynamics. This is considered through a concept of reduced design and analysis complexity that makes the vehicle comparable to a bouncing ball. Kovač used a similar concept to ensure the hopper passively regain its attitude after landing [11].

At the opposite end of the scale, hopper designs have been proposed that make use of a rocket powered system [2, 12–14]. Amongst these, the use of in-situ resources is very popular for Mars based concepts: CO_2 rich Martian atmosphere can be used as propellant with a thermodynamic cycle to energise it. Although this gas-rocket-based design provides long range hopping capabilities (in the order of kilometers for the references quoted), it does not allow short range mobility and the powered transition to aerial stage absorbs a substantial

amount of energy.

Jumping mechanisms, coupled with devices extending the flight time, have been proposed in the framework of “jump-gliding” dynamics, often linked to bio-inspired concepts. This is the case of MultiMo-Bat [15] where a spring mechanism produces a ballistic jump and the range is extended by means of wing spreading as the mechanism unfolds. Along the same lines, Kocač [16] assesses the advantages of jump-gliding compared as simple jumping dynamics. Finally, the work by Desbiens *et al.* [17] proposes design guidelines for the jump-gliding approach analysing the dynamics of two hoppers of this sort. It is clear from the references cited above that hopper designs based on coupling ballistic jumps with devices to enhance the flight utilise gliding concepts. No design has been considered as a viable alternative in the case of flight in vacuum conditions or whenever the medium (atmosphere) characteristics do not allow for the exploitation of aerodynamic effects. On one end rockets designs have been presented with dynamics independent of the leg propulsive aid, on the other, when legs are considered the aerial motion is either ballistic or aided through aerodynamics means. It is then interesting to investigate how, taking advantage of the leg dynamics to start the aerial stage, a hopper can be designed with the ability of extending its range through active propulsion. This would increase the controllability of the hopper with the advantage, amongst the others, of facilitating the selection of the landing site. Moreover, this would improve the robustness of a space exploration hopper by excluding the uncertainty linked to the aerodynamics of the glided flight in an extra-terrestrial atmosphere.

This paper focusses on a hopper design featuring active legs, capable of projecting the vehicle into the aerial stage. To this end, the design of the vehicle is based on the physiology of the locust legs. Locusts contract their hind legs and store energy in an elastic tissue known as “semilunar process” [18]. This

is then released in the final phase of the leg extension for the jump, with the neural system triggering the activation sequence through electrical pulses [19]. A realisation of such a concept has been attempted by Birch *et al.* with the resulting robot able to coordinate forward and hind legs to advance, without, anyway reproducing the long jumps typical of crickets and locusts [20,21]. More recently, locust inspired robots have been considered and studied in terms of performance, see for example [22–24], which highlight how timely this theme is. A modelling approach is used which is similar, and in some respect complementary, to the one used by Bonsignori *et al.* [25], who considered the *Cicadella Viridis* and studied the jump dynamics connecting the geometry of the legs to some characteristics of the acceleration. This approach involves the synthesis of some key features of the locust leg (mainly geometry, mass distribution and kinematics) with a simple mass-spring model. We show that it is in theory possible to retrieve the key characteristics of the locust jump with engineering artefacts. Our analysis extends to include scaling up towards sizes of interest from the mechanical design point of view. In the same spirit, the flight stage is considered as a design optimisation problem looking at the optimal direction of a constant thrust vector to achieve maximum range.

The engineering of such a device is studied through substituting the muscles and the semilunar process with elastic elements, e.g. springs. The result is a simplified model which is compared to the biological data obtained from observing the hopping characteristics of locusts. Analysis of the proposed design is illustrated in this paper via the development of analytic models. The motion is broken into three stages i.e. pre-launch, launch and aerial. The landing stage is not considered as a complete analysis would expand beyond reason the scope of this work; this topic is however considered in the Discussion. The launch stage is divided in two phases. The development of these models is based on appro-

priate Euler-Lagrange representations. Key design parameters for this system are developed based on desired performance requirements, biological data and a backward integration process. These parameters and mathematical models are used in numerical simulations to obtain response data for the system. Through modelling, design and setting parameters are here defined using an accessible mathematical development. These include the stiffness of the elastic elements and the initial setting angles in the pre-launch stage. The launch angle, defined to meet the desired range, is here shown to be obtainable considering the magnitude and the direction of the thrust vector. The range is proved to be maximised for the launch velocity parallel to the thrust vector, in case this is constant throughout the aerial stage. These results are analysed and discussed in depth in the latter part of this paper. Finally, conclusions drawn from the results of this study are presented as a finale to this paper.

2 Derivation of Hopper Dynamics in the Launch Stage

The hop dynamics are obtained by considering the vehicle as connected point masses with a total of three degrees of freedom. These are activated by linear springs. Fig. 1 shows the geometry of the concept considered with the notation used. The model simplifies the locust jumping legs through a single leg device and the motion is considered in the vertical plane only.

As previously discussed, the dynamics of the hopper can be considered as three separate stages, i.e. pre-launch, launch and aerial, which replicate the hopping gait of a locust. These are shown in the schematic of Figure 2. The conditions to set the system at the end of the pre-launch stage are derived

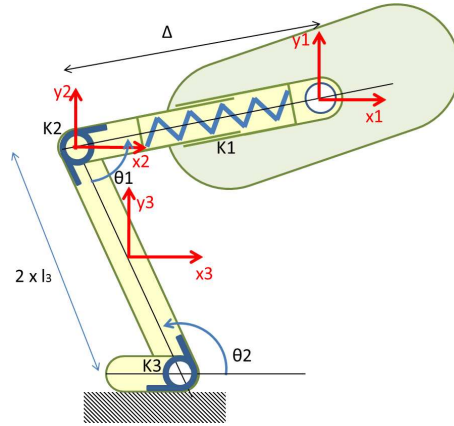


Figure 1: Hopper scheme. The sketch shows the general arrangement of the lumped masses and springs used to model the locust leg. The centres of mass of the different bodies correspond to the origin of the local reference frames. k_1 , k_2 and k_3 are indicate the springs with k_2 represented as a torsional spring although the case of an in-line spring is considered too. A prismatic connection exist between the two ends of the femur allowing for the extension of k_1 spring. Angles are considered positive counter-clockwise, as arrows indicate.

through the analysis of the launch and the aerial stages. In order to reproduce these dynamics the physiological aspects of locust legs are considered. Within this framework the leg geometry can be approximated in two ways based on different representations of the femur-tibia joint. In the first case this is represented by linear torsional spring, in the second, an in-line spring stretches from the femur to an extension of the tibia. The two schemes are shown in Fig. 3. Both are modelled to isolate the advantages of a more faithful biomimetic design or a more compact one. The in-line spring assembly is closer to the actual geometry of a locust leg, with a *mechanical advantage* originated by the variable lever arm during the rotation, but this design implies an in-line spring, stretching between the femur and the tibia extension. Note that, at this level of analysis there is no difference in considering the tibia metothoracic or mesothoracic, that is, considering the angle between the tibia and its extension [19].

More in detail, the launch stage is modelled considering the following main

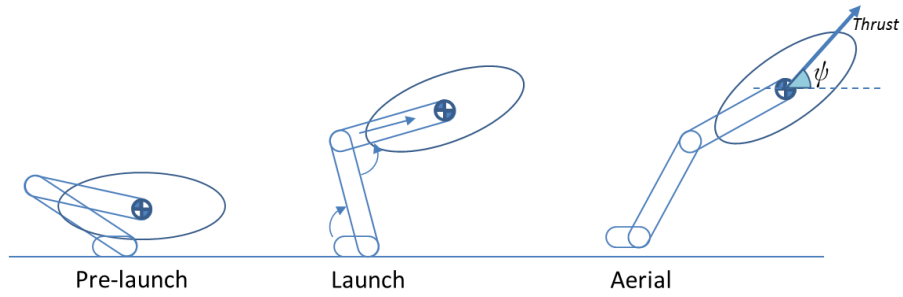


Figure 2: Stages of the Jump. In the Pre-launch stage the legs are contracted and muscles are “loaded”. In the Launch stage legs are extended and, by result, the body parts acquire momentum as indicated by the arrows. Finally, in the aerial phase, locusts motion is aided by wings, whilst in this context constant thrust, at an angle ψ with respect to the horizontal, is considered.

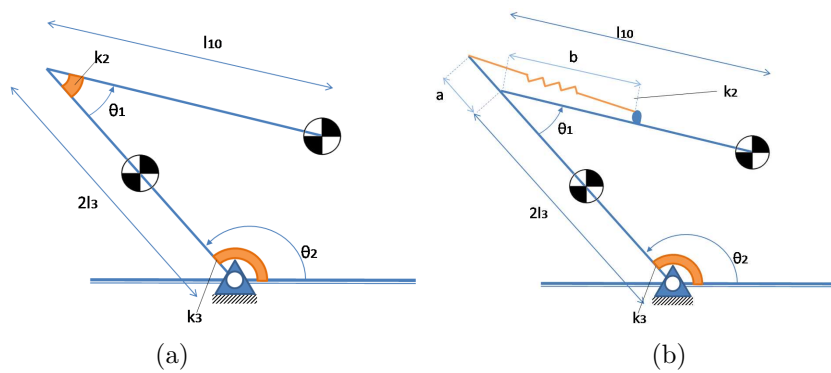


Figure 3: Phase 1 schematic. Torsional springs are here represented as circular bands. The centres of mass considered in this phase are indicated by the popular 2-colour circles.

assumptions:

- The model is non-dissipative and the motion happens in absence of dissipative forces;
- the motion is confined to the vertical plane;
- the motion is divided in two phases with two out of the degrees of freedom involved in each: this makes the system a two-body system in each of the phases;
- there is no slip in the contact between the foot and the ground;
- each of the parts of the multi-body system is perfectly rigid and are considered as lumped masses.

For any set of generic n coordinates ξ_i of the system with $i \in \{1\dots n\}$, and in absence of dissipative terms, the Euler-Lagrange Equations are defined as

$$\frac{d}{dt} \left(\frac{\partial K_e}{\partial \dot{\xi}_i} \right) - \frac{\partial V}{\partial \xi_i} = 0 \quad (1)$$

where, K_e and V are the kinetic and potential energy of the system respectively. The kinematic relations linking the point mass coordinates to the system chosen frame are

$$\begin{aligned} x_1 &= 2l_3 \cos \theta_2 - \Delta \cos(\theta_1 + \theta_2) \\ y_1 &= 2l_3 \sin \theta_2 - \Delta \sin(\theta_1 + \theta_2) \\ x_2 &= 2l_3 \cos \theta_2 \\ y_2 &= 2l_3 \sin \theta_2 \\ x_3 &= l_3 \cos \theta_2 \\ y_3 &= l_3 \sin \theta_2 \end{aligned} \quad (2)$$

The set of Equations (2) put in relations the three local reference frames, which are centred on the body centre of mass (1), the femur-tibia joint (2) and the tibia mid point (3). Moreover, as illustrated in Fig. 1, $2l_3$ is the tibia length, θ_1 and θ_2 are the angles between the femur and the tibia and between the tibia and the horizontal plane, respectively. They are taken positive counter-clockwise.

The launch stage is broken into two phases, reflecting the activation sequence of the locust and grasshopper hind legs. In the first phase the angular joints are operated to extend the leg in a suitable direction and gaining momentum for the final kick. This is provided in the second phase, which is triggered by the full extension of the θ_1 degree of freedom to 150° , in accordance with [18]. The actual kick is provided by the linear spring k_1 , which, for the purpose of this study, substitutes the semilunar process of a real locust. The second phase ends when the linear spring reaches its natural extension. Note that spring k_1 is released only when the femur-tibia joint is at full extension. This is necessary due to the lack of control for the torque in the extension of the femur-tibia joint, a simplification introduced in the engineering model. In real locusts, the semilunar process starts unfurling when the femur-tibia joint is in motion. However, the torque in the joint has to increase in response to the additional load brought by the semilunar process. The leg rotation and the unfurling of the semilunar process end at the same time [26]. However, having the femur-tibia joint activated by a simple spring prevents to increase the torque, when needed, to contrast the action of the spring k_1 . The release of k_1 is hence delayed until the joint is completely extended and locked.

The presence of a spring k_3 at the tibia-foot joint is considered, despite most studies in the relevant biological literature neglect its contribution to the locust jump. This is possibly because it has a control function only, providing negligible momentum compared to the other springs. This is reflected by the stiffness

associated to it in this work. From the engineering point of view, k_3 prevents the tibia from collapsing backward while building up the momentum, provides progression in the rotation, beside being sensible from the biological point of view.

2.1 Launch Stage - First Phase

The first phase involves the rotational degrees of freedom θ_1 and θ_2 . The schematic of this first phase is shown in Fig. 3 for the two configurations considered. The lumped masses 1 and 2, representing the body and the femur, respectively, are considered as one with a centre of gravity at the insertion of the femur on the body. This is acceptable as the two masses do not change relative positions and the body is substantially larger than the femur. The first phase ends when joint 1 gets fully extended, that is, θ_1 reaches and locks at $\theta_{1fin} = 150^\circ$. In case of a torsional spring at femur-tibia joint, the kinetic and potential energy associated with the motion in this phase are

$$K_e = \frac{1}{2} [m_{12}(\dot{x}_1^2 + \dot{y}_1^2) + m_3(\dot{x}_3^2 + \dot{y}_3^2)] \quad (3)$$

$$V = \frac{1}{2} [k_3(\theta_2 - \theta_{20})^2 + k_2(\theta_1 - \theta_{10})^2] + m_{12}gy_1 + m_3gy_3 \quad (4)$$

where, $m_{12} = m_1 + m_2$, θ_{10} and θ_{20} are the values the angles take when the respective springs are unloaded. Through the kinematic relationships (2) the kinetic and potential energies can be expressed as

$$\begin{aligned} K_e &= \frac{1}{2} m_{12} \left[4l_3^2 \dot{\theta}_2^2 + l_{10}^2 (\dot{\theta}_1 + \dot{\theta}_2)^2 - 4l_{10}l_3 \dot{\theta}_2 (\dot{\theta}_1 + \dot{\theta}_2) \cos \theta_1 \right] + \frac{1}{2} m_3 l_3^2 \dot{\theta}_2^2 \\ V &= \frac{1}{2} [k_3(\theta_2 - \theta_{20})^2 + k_2(\theta_1 - \theta_{10})^2] \\ &+ m_{12}g [2l_3 \sin \theta_2 - l_1 \sin(\theta_1 + \theta_2)] + m_3 g l_3 \sin \theta_2 \end{aligned} \quad (6)$$

where, l_{10} is the length of the femur segment when the spring k_1 is compressed. The case of an in-line spring between an extension of the tibia of length a and a point on the femur at distance b from the femur-tibia joint is shown in Fig. 3.b, the kinetic and potential energy associated to the motion in this phase are

$$K_e = \frac{1}{2} [m_{12}(\dot{x}_1^2 + \dot{y}_1^2) + m_3(\dot{x}_3^2 + \dot{y}_3^2)] \quad (7)$$

$$V = \frac{1}{2} [k_3(\theta_2 - \theta_{20})^2 + k_2(\delta - \delta_0)^2] + m_{12}gy_1 + m_3gy_3 \quad (8)$$

where, $\delta = \sqrt{a^2 + b^2 + ab \cos \theta_1}$ and δ_0 is the value δ takes at the end of the first phase, corresponding to the unloaded length of the k_2 spring.

The final forms of the Euler-Lagrange equations for the first phase are reported in the Supplementary Materials S1.

2.2 Launch Stage - Second Phase

The second phase starts as soon as the femur-tibia joint reaches and locks at 150° angle. The coordinates considered in this phase are the angle θ_2 and the extension Δ which is triggered by the locking of θ_1 . The model in this second phase considers the lumped masses 2 and 3 as a single one with common centre of gravity on the femur-tibia joint. This can be accepted as the two masses do not change their relative position during this phase. Moreover, the femur and the tibia have comparable masses according to the biological measurements considered (see Section 4.3). This is pictured in the schematic of Fig. 4. The kinetic and potential energy are given by

$$K_e = \frac{1}{2} [(m_2 + m_3)(\dot{x}_2^2 + \dot{y}_2^2) + m_1(\dot{x}_1^2 + \dot{y}_1^2)] \quad (9)$$

$$V = \frac{1}{2} [k_3(\theta_2 - \theta_{20})^2 + k_1(\Delta - \Delta_0)^2] + (m_2 + m_3)gy_2 + m_1gy_1 \quad (10)$$

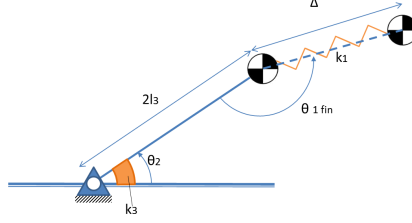


Figure 4: Phase 2 schematic. The torsional springs k_3 is represented as a circular band. The centres of mass considered in this phase are indicated by the popular 2-colour circles. θ_1 is locked in this phase at its final value.

where Δ_0 is the uncompressed length of spring k_1 . Through the kinematic relations (2) the kinetic and potential energies can be expressed as

$$K_e = \frac{1}{2}m_1 \left[\dot{\Delta}^2 + (2l_3 + \Delta)^2 \dot{\theta}_2^2 \right] + (m_1 + m_3)2l_3^2 \dot{\theta}_2^2 \quad (11)$$

$$V = \frac{1}{2} \left[k_3(\theta_2 - \theta_{20})^2 + k_1(\Delta - \Delta_0)^2 \right] + 2(m_2 + m_3)gl_3 \sin \theta_2 + m_1g(2l_3 + \Delta)\sin(\theta_2) \quad (12)$$

Through Eq. (1) the Euler-Lagrange equations for the second phase can be obtained and these are reported in the Supplementary Materials S2.

3 Aerial Stage

The Aerial stage can be ballistic or powered. Both of them are covered for the drag-free case. While for the ballistic case a simple algebraic development can be used, for the powered case, differential relations have to be considered. However, as the ballistic case can be considered a special case of the powered one, its development is detailed in the Supplementary Materials S3. When variable thrust, in magnitude and direction, is considered, then the maximum range problem has to be undertaken through variational methods. These are not considered here. The aerial stage is modelled considering the following assumptions:

- The model is non-dissipative and the motion happens in absence of dissipative forces;
- the motion is confined to the vertical plane;
- the joints of the multi-body system lock at lift-off and the whole system is perfectly rigid for the whole duration of the aerial stage.

The equations of motion for the powered aerial stage in the vertical plane are:

$$\begin{aligned}\ddot{x} &= T \cos \psi \\ \ddot{y} &= T \sin \psi - g\end{aligned}\tag{13}$$

where, T is the acceleration provided by any force (e.g. thrust, lift) acting at an angle ψ with respect to the horizontal axis. This is considered constant during the flight. Note that, given the point mass model for the flight stage, it is possible to scale all the forces by the system mass and hence work only with the accelerations. The range for the powered flight can be obtained by integrating twice the Eqs. (13) with initial velocity v_L at an angle Θ with respect to the horizontal axis and initial position in the origin. This returns

$$R = \frac{1}{2}T \cos \psi t_f^2 + v_L \cos \Theta t_f\tag{14}$$

$$y = \frac{1}{2}(T \sin \psi - g)t_f^2 + v_L \sin \Theta t_f \quad .\tag{15}$$

The flight time t_f can be obtained from Eq. (15) for $y = 0$ assumed as the landing height. Excluding the trivial solution $t_f = 0$, it returns

$$t_f = -\frac{2v_L \sin \Theta}{T \sin \Theta - g} \quad .\tag{16}$$

Substituting Eq. (16) into Eq. (14), the range becomes

$$R = \frac{1}{2}T \cos \psi \frac{4v_L^2 \sin^2 \Theta}{(T \sin \psi - g)^2} - \frac{2v_L^2 \cos \Theta \sin \Theta}{T \sin \psi - g} . \quad (17)$$

The maximum range can be found in this conditions by simply taking the partial derivatives of Eq. (17) with respect to the variables Θ , ψ and T and imposing these to be identically null at the same time.

$$\begin{aligned} \frac{\partial R}{\partial \Theta} &= \frac{2Tv_L^2 \cos \psi}{(T \sin \psi - g)^2} \sin(2\Theta) - \frac{2v_L^2}{T \sin \psi - g} \cos(2\Theta) = 0 \\ \frac{\partial R}{\partial \psi} &= -\frac{4T^2 v_L^2 \sin^2 \Theta \cos^2 \psi}{(T \sin \psi - g)^3} + \frac{2Tv_L^2 \sin \Theta \cos(\Theta + \psi)}{(T \sin \psi - g)^2} = 0 \\ \frac{\partial R}{\partial T} &= \frac{2v_L^2 \sin^2 \Theta \cos \psi [(T \sin \psi - g) - 2T \sin \psi]}{(T \sin \psi - g)^3} + \frac{v_L^2 \sin(2\Theta) T \sin \psi}{(T \sin \psi - g)^2} = 0 \end{aligned} \quad (18)$$

By inspection, it can be seen that the derivative with respect to T is always positive for $\Theta, \psi \in]0, \pi/2[$ and $T < g$, that is, the range is an always increasing function of the thrust. The same could be trivially said about the initial launch speed v_L , although not shown here. The derivative with respect to Θ instead is null for

$$\Theta = \frac{1}{2} \tan^{-1} \left(\frac{T \sin \psi - g}{T \cos \psi} \right) + n \frac{\pi}{2} \quad (19)$$

where, $n \in \mathbb{Z}$ accounts for periodicity. A value of $n = 1$ returns an angle Θ in the interval $[0, \pi/2]$. In case $\Theta = \psi$, that is the thrust is parallel to the initial velocity vector, the angle Θ maximizing the range reduces to

$$\Theta = \sin^{-1} \left(\frac{\frac{T}{g} + \sqrt{8 + \frac{T}{g}}}{4} \right) . \quad (20)$$

For any other value of $\psi \neq \Theta$, Eq. (19) can be substituted into the second

of Eqs. (18) and the resulting expression solved numerically. However it can be proved that, for Θ defined by Eq. (19), the range is maximised for $\Theta = \psi$ (Supplementary Materials S4 and S5). This makes the optimal ψ elegantly obtainable from Eq. (20). The values of Θ and ψ maximising the range are hence function of the thrust and gravitational acceleration only.

4 Backward Integration and Parameter Mapping

The initial setting of the elastic elements producing a desired ballistic or powered jump is obtained through backward integration. This is a technique through which the time history of a dynamical system is obtained starting from the final conditions, rather than the initial ones. The final conditions used in this work are the conditions at lift-off. These are determined by the desired trajectory. In particular, for a trajectory that maximises the range, the take off angle is defined by Eq. (19) depending on the ballistic or powered flight conditions. The resulting time history of the leg extension is compared with the biological data after the mass and the stiffness have been traced down to their corresponding quantities in the locust physiology. This is done for the lift-off angle that maximises the range in the ballistic case. This is to verify the lumped mass and spring model is a faithful representation of the dynamics of the locust hop, the model output. To this end, the measurement in [18, 19, 26] are considered.

4.1 Final Conditions for the Backward Integration

The lift-off velocity is defined as the vector sum of the velocity produced by the extension of the k_1 spring and the one induced by the rate $\dot{\theta}_{2fin}$. Through the

cosine law this is defined as

$$v_{des} = \sqrt{\dot{\Delta}_{fin}^2 + \sigma^2 + 2\dot{\Delta}_{fin}\sigma \sin(\theta_{1fin})} \quad (21)$$

where $\sigma = (2l_3 + l_1 \cos(\theta_{1fin}))\dot{\theta}_{2fin}$. Equation (21) can be solved for $\dot{\Delta}_{fin}$ to define the final extension rate of the semilunar process, once the magnitude of the desired take-off velocity v_{des} is set. The final length reached by the semilunar process extends the femur to its given length. This implies that the compression of the semilunar process modifies the geometry of the mechanism, which is reflected in the equations of motion being dynamically coupled.

The final launch angle Θ_{des} is the angle of the speed vector with respect to the horizon at the end of the second phase. This is the sum with sign of the angles θ_2 and the complement of θ_1 to π , but also includes the angle induced by the θ_2 rate of change. Θ_{des} is expressed as

$$\Theta_{des} = \theta_{2fin} - (\pi - \theta_{1fin}) + \tan^{-1} \left(\frac{-v_{\theta 2} \cos(\theta_{1fin})}{\dot{\Delta}_{fin} + v_{\theta 2} \sin(\theta_{1fin})} \right) \quad (22)$$

where, $v_{\theta 2} = \dot{\theta}_{2fin}(2l_3 - l_1 \cos(\theta_{1fin}))$ is the linear velocity at the end of the femur induced by the angular rate $\dot{\theta}_{2fin}$. $\theta_{1fin} = 150^\circ$ is the final angle of the femur-tibia joint, $\dot{\theta}_{2fin}$ is the final angular rate of the tibia-foot joint and θ_{2fin} is the final angle of the tibia-foot joint needed to achieve an initial launch angle Θ_{des} . This is set to -1 rad/s based on the data found in [26] showing nonzero angular rate at lift-off, yet much smaller than the average one throughout the extension. The data in [26], however, refer to the femur-tibia joint which is here assumed extending at the same speed of the tibia-foot joint, although, in the present setting, the femur-tibia joint is already locked at lift-off.

Equation (22) can be solved for θ_{2fin} to define uniquely the final value of the angle for a given desired inclination of the launch speed vector Θ_{des} , and the

final value of the semilunar process speed, with the other parameters fixed.

The final extension of the femur-tibia joint is set to 150° , as already stated, compliant with the literature. Its final angular rate $\dot{\theta}_{1fin}$ is set equal to the instantaneous angular rate of the tibia-foot joint at the same time instant, that is, at the end of the first phase.

The stopping conditions for the backward integrations are the achievement of a null extension rates $\dot{\Delta}$ and $\dot{\theta}_1$ respectively for the second and first phase. $\dot{\Delta} = 0$ produces the switch from the second to the first phase and $\dot{\theta}_1 = 0$ is the condition to conclude the backward integration of the first phase and of the whole dynamics.

4.2 Lengths

Lengths of the legs are taken from the measurement in [18] that reports similar lengths for the femur and the tibia of about 24-25 mm. Consistently the femur and tibia lengths are chosen as 24 mm. With reference to Fig. 3.b, length a is considered 0.37mm as measured by Bennet-Clark [18]. Length b is not reported in the relevant biological literature as the extensor muscle exerts a force along all the length of the femur. However, wise engineering implementation would recommend to reduce the burden of the elastic elements. For this reason b length has been set to 1 mm.

4.3 Masses

The locust population analysed by Bennet-Clark [18] features a mass of 1.5-2.0 grams for male locusts and 2.5-3.5 grams for females. The values found in [27] do not differ significantly from these values. In this work a total mass 2.8 grams was chosen. This was subdivided as 2.2 grams for the body (m_1), 0.3 grams for each femur (m_2) and 0.1 grams for each tibia and foot (m_3). Just half of the

body mass is considered for the calculation. This is because locusts use both legs in a symmetric way to power the jump.

4.4 Spring Stiffness

By comparing the extensor muscle and the semilunar process to linear springs, Bennet-Clark produced stress-strains relation with average slopes close to 20 N/mm and 40 N/mm. While the value for the semilunar process is obtained through a mechanical test, the stiffness of the spring mimicking the extensor muscle derives from more complicated tests, which also produced deformations in the semilunar process. The values obtained are sensibly higher than other examples in the literature, for example Heitler [19], as admitted by the author himself [18]. For this reason, while keeping the value of 40 N/mm for the semilunar process, the compression spring replacing the extensor muscle is given a stiffness of 1 N/mm, which returns a time duration of the leg extension closer to the biological data. To map this to the model where the extensor muscle is replaced by a torsional spring in the femur-tibia articulation, it is considered that the amount of energy stored in the springs must be the same. Hence,

$$\frac{1}{2}k_{2comp} \left(\sqrt{a^2 + b^2 - ab \cos(\pi - \theta_{1ini})} - \delta_0 \right)^2 = \frac{1}{2}k_{2tors} (\theta_{1ini} - \theta_{1fin})^2 \quad (23)$$

where, k_{2comp} and k_{2tors} are the stiffness of the compression and the torsional spring, respectively. Subscripts “*ini*” and “*fin*” refer to the initial and final values of the variables. As previously stated, k_{2comp} is given the value of 1 N/mm. Solving Eq. (23) for k_{2tors} , considering $\theta_{1ini} = \pi/4$ returns $k_{2tors} = 9.810^{-9} Nmmrad^{-1}$.

The value of k_3 is chosen so to use the tibia-foot torsional spring to balance the action of the femur-tibia joint. Suitable values for k_3 stiffness depend on the stiffness values of the other springs; in particular, the plots in Fig. 5 refer

to the case of $k_3 = 0.005Nmrad^{-1}$. The choice of the neutral angle for this joint (the angle at which the spring k_3 is unloaded) follows from the same attempt of balancing the whole movement. The value of 120° chosen seems however quite close to what can be considered a natural resting position of the leg, although it was not possible to validate this against some reference in the literature. The neutral angle for the femur-tibia joint is instead set to 150° , which also corresponds to the maximum extension considered for the joint. This corresponds to assuming the momentum in the extension of the joint is maximum at the end of the first phase, as it is reasonable to expect. Neutral angles have no correspondence in the biological original, however they are needed because of the modelling technique used.

5 Scaling up for typical robot-size devices

The Biological similitude unlocks the design of a mechanical device that uses rods and springs to emulate locust leg. However, the size of the hopper robots realised nowadays are in the order of decimetres, while the maximum length for the biological examples considered here are not larger than 25 mm. This makes scaling necessary to provide meaningful direction towards the design of a robotic hopper.

The literature in the field proposes several scaling approaches, some better suited than others depending on the application [28]. For this particular case we considered two possible scaling techniques. They both rely on accelerations remaining unchanged as gravitational environment does not depend on the size of the robot. This is to say, as gravity cannot be scaled, all the accelerations the robot undergoes shall be retained in the scaled model. With this assumption, the approach followed by Rastogi *et al.* [29] considers also the Young module of the material to stay the same being their study developed in a structural

dynamics framework. According to this method, if N is the scaling factor, all the linear lengths are scaled by N and times by \sqrt{N} , which return no scaling for the accelerations, as previously discussed. Force and mass are scaled by N^2 as mass density is scaled by N^{-1} . This approach returns spring stiffness scaled by N .

Alongside the approach by Rastogi *et al.*, we also consider a density conserving approach where linear lengths are still scaled by N , but, to keep density constant, mass is scaled by N^3 . This implies time and velocity to be scaled by $N^{1/2}$. Results obtained by scaling the mechanisms through these techniques are reported in Section 6 and discussed in Section 7.

6 Numerical Integrations

6.1 Biological Comparison

The dynamics are numerically integrated for both models considered in the first phase (i.e. two torsional springs or one torsional and one in-line spring), from the take-off time, backwards using a DormandPrince routine with variable time step. Both models track well the data in the relevant biological literature.

Figure 5 shows the time history of the three degrees of freedom for both the models considered. The time span over which the mechanism unfold matches quite closely the data reported in [18] and [26]. This also applies for the conditions at the beginning of the extension movement, which, because of the backward integration, are an output of the model. Bennet-Clark [18] reports an initial angle of the femur-tibia joint around 15° and an unfurling of the semilunar process of 0.3-0.4 mm. With a final lift-off angle of 45° and a final take-off speed of 2.5 m/s [18], the model predicts an initial angle at the femur-tibia joint of 44.5° for the model with the in-line spring and 46.4° for the model comprising a

torsional spring and the femur-tibia joint. In Fig. 5 the effect of the mechanical advantage is visible in the initially slower spreading of all the degrees freedom. In particular, in Fig 5.b θ_1 takes longer to deploy with the in-line spring. It then matches and, in the central part of the plot, anticipates the deployment of the system with the torsional spring. By design, both systems deliver the same final angle and final rate.

6.2 Performance of the Scaled System

The simulations presented in the previous section were repeated for the model scaled according to the methods discussed in Section 5. For both the scaling methods proposed, the linear sizes were scaled by 5, 10 and 50 times, with the other physical parameters scaled as consequence. This, compared with the biological data, leads to consider a hopping robot from 10 cm to approximately 1 metre in length. For brevity, only the $\times 10$ case is illustrated here in Fig. 6. The $\times 5$ and $\times 50$ scaled cases are reported in the Supplementary Materials, Section S6. The plots show how the scaling conserves the trend of the biological comparison just when a torsional spring is used in the femur-tibia joint. This is independent from the scaling technique used. The scaling of the system with an in-line spring, instead, shows a different trend. Further considerations about the scaled system are provided in the Discussion, Section 7.

6.3 Simulation of the Aerial Stage

The effects of the thrust on the range in the aerial stage are illustrated in Figs. 7 and 8. Both figures are obtained considering a single point mass located at the femur-body joint, which represent the main body section of the insect. The plots in Fig. 7 show that the optimal launch angle is a nonlinear function of

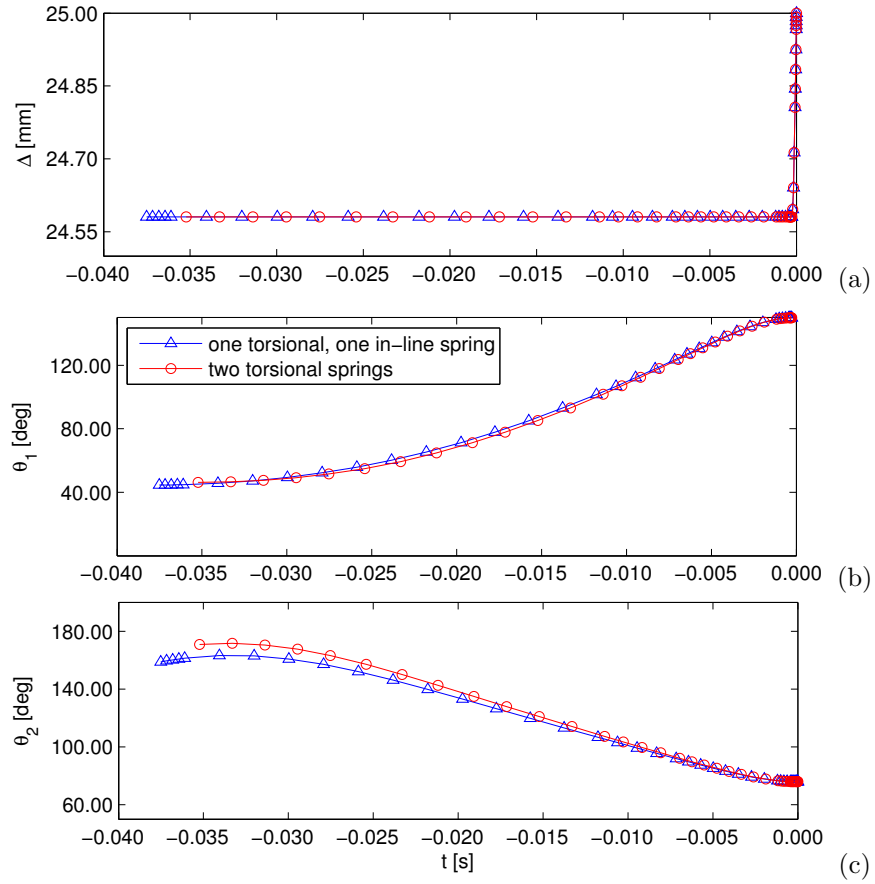


Figure 5: Time history of the system's degrees of freedom for the model with two torsional springs (red circles) and the model with one torsional and one in-line spring (blue triangles). (a) extension of the spring k_1 , mimicking the semilunar process (Δ); (b) relaxation of the spring k_2 at the femur-tibia joint (θ_1); (c) relaxation of the spring k_3 at the tibia-foot joint (θ_2). The end of the second phase, that is, the lift-off time, is considered as the zero of the time axis.

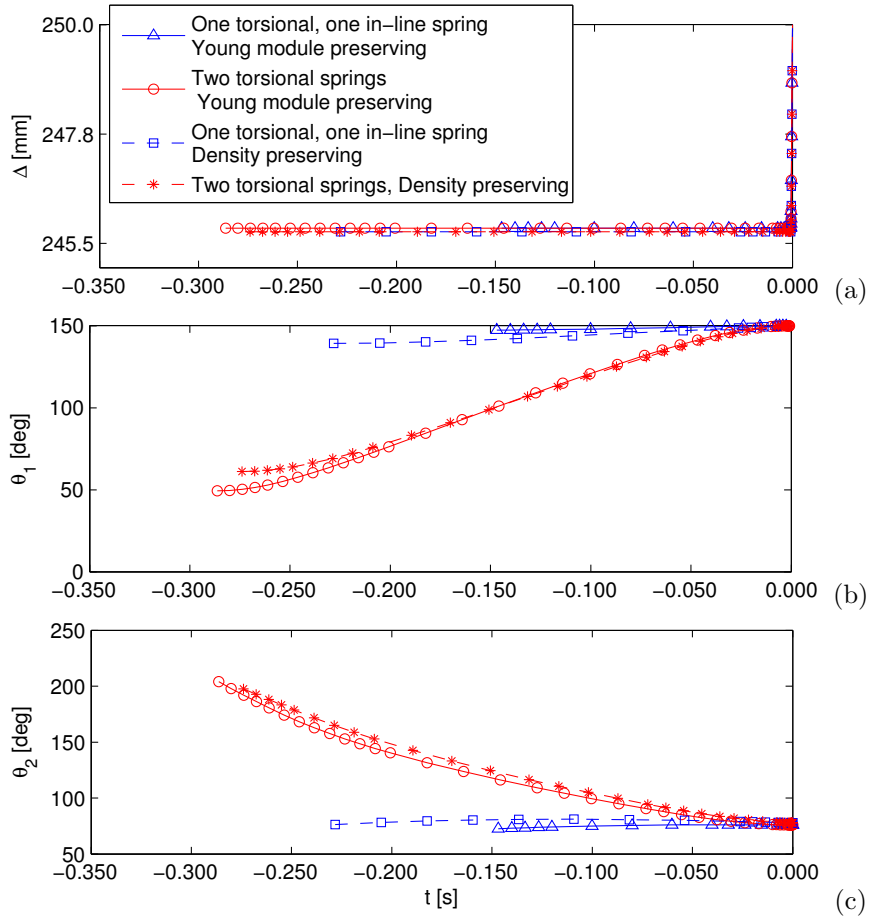


Figure 6: Time history of the system's degrees of freedom for the model scaled ten times. (a) extension of the spring k_1 , mimicking the semilunar process (Δ); (b) relaxation of the spring k_2 at the femur-tibia joint (θ_2); (c) relaxation of the spring k_3 at the tibia-foot joint (θ_2). The end of the second phase, that is, the lift-off time, is considered as the zero of the time axis.

the thrust angle. This is described by Eq. (19). The contour plots are reported for 4 magnitudes of the thrust-resulting acceleration, accounted as fractions of the gravity acceleration. For null thrust, Fig. 7.a, the purely ballistic case for which the optimal launch angle is independent from ψ and is equal to 45° . As the magnitude of the thrust increases, the optimal ψ angle is obtained for the thrust aligned to the launch angle, matching the value predicted by Eq. (20). This is confirmed by the position of the maximum moving along the diagonal as thrust increases from figure 7.b to d. For the same range of thrust magnitudes Fig. 8 shows the trajectories in the $x - y$ plane for the optimal launch angle, that is $\Theta = \psi$ obtainable from Eq. (20) and a take-off speed of 2.5 m/s, typical of real locusts.

As thrust is considered on in relation to gravity accelerations, the analysis of the aerial stage is not repeated for the scaled-up model. This would differ just for the magnitude of the initial, take-off velocity: as discussed in Section 3, a higher initial velocity would simply scale up the range without changing the optimal launch angle.

7 Discussion

This work presented the engineering of a mechanical jumping system inspired by locusts, relying on the sequential activation of springs with different stiffness. This is done with the clear intent of exploring possible hopper design characterised by long, ballistic hops, to which thrusting devices can be optionally added to extend the flying stage. As such, this work proposes a concept that inserts in the gap between gait-mimicking devices and hoppers often proposed as means for planetary exploration in the literature.

The effectiveness of the engineering synthesis was evaluated by comparing the performance obtained with the biological data about locust jump found in the

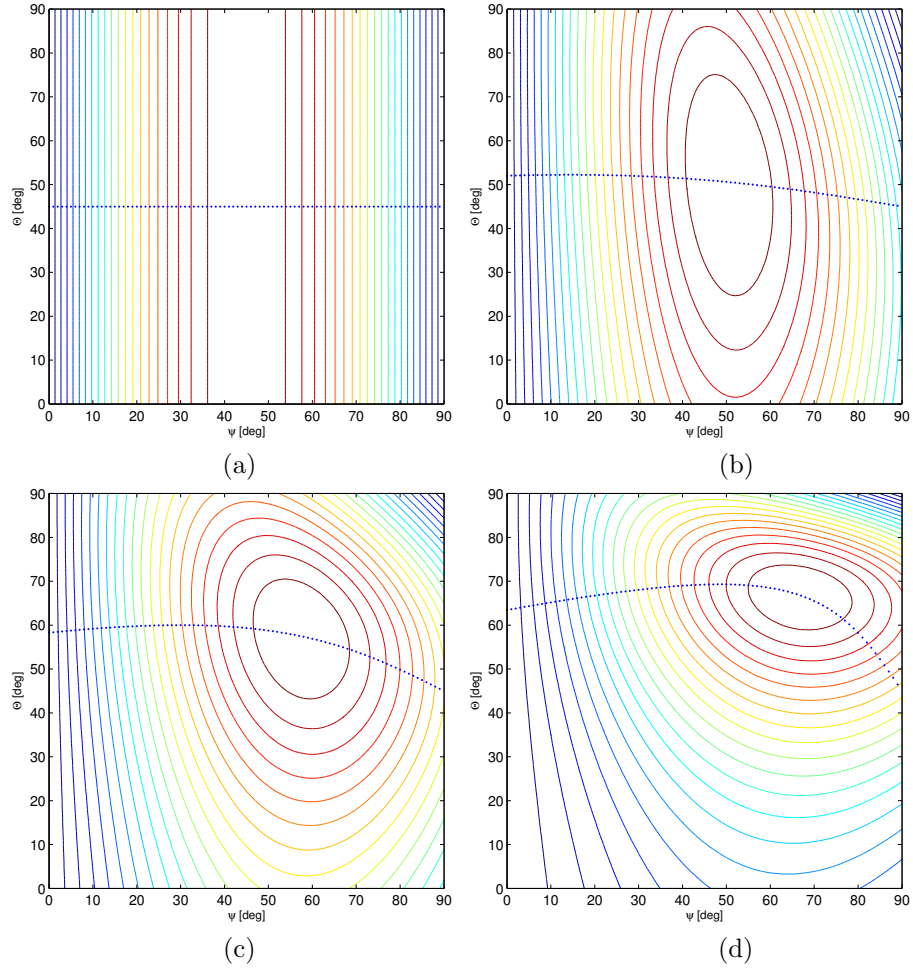


Figure 7: Range contours for take-off angle Θ and thrust direction ψ , for four values of the thrust magnitude. (a) Ballistic case; (b) Thrust acceleration magnitude is $1/4$ of the gravitational acceleration; (c) Thrust acceleration magnitude is half of the gravitational acceleration; (d) Thrust acceleration is $3/4$ of the gravitational acceleration in magnitude. The dotted line is the solution of Eq. (19)

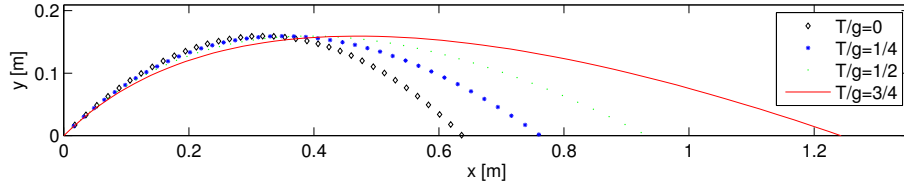


Figure 8: Trajectory in the $x - y$ plane for four values of the thrust to gravitational acceleration ratio at the optimum thrust and launching angle $\Theta = \psi$ from Eq. (20)

literature. Data in [18], [19] and [26] are in line with the results reported here. Despite the crude simplification of reducing muscles to a series of pre-loaded springs, the main features of locust jump are retained. In particular, the time history of the femur-tibia joint reproduces nicely the data in [18] and [26]. However, some expedients were necessary to account for the lack of control in the relaxation of preloaded springs, as opposed to what real muscles provide. Of these, the most important one is the subdivision of the movement in two phases with the femur-tibia joint locked at the end of the first one. This is not what happens in locust leg where the joint continues the extension, which ends when also the semilunar process is fully unfurled. The relaxation of the k_1 spring with the femur-tibia joint not locked, would produce the contraction of the θ_1 degree of freedom, unless this would be counteracted by a torque feedback device. This, due to the minimalist approach chosen, cannot be realised through the preloaded springs.

Another deviation from the biological example was operated at the tibia-foot joint, which was provided with a torsional spring. This has the effect of balancing the femur-tibia joint conferring progression in the joint relaxation. To this end, the zero torsion angle of the tibia-foot joint has to be suitably set. The time history of the tibia-foot joint alternates stretch and compression phases during which the foot is assumed to keep contact with the ground. To the author best

knowledge, there are no data in the biological literature about the mechanical properties of the tibia-foot joint that could confirm or rule out the balancing role assumed here. Considering the tibia-foot joint was necessary to overcome the limitation of the minimalist design presented here, just relying on springs activated in sequence. The attaching point of the femur spring for the model where the femur-tibia joint is activated by a compression spring was not selected on the basis of the biological equivalent. Heitler [19] only provides the distance from the joint at which the muscle is attached on the tibia extension. The extensor muscle stretches along the whole femur as opposed to a spring which, for design reason, may be chosen to be shorter. This determined the choice of considering the spring attached at 1 mm from the femur-tibia joint. This choice, however, influences the dynamics of the joint extension as it changes the time history of the levering arm length, the so-called “mechanical advantage” [18, 19, 27].

The stiffness of the springs are defined considering measurements of locust tissues’ mechanical properties. The contraction lengths confirm the validity of the choice. The semilunar process is reported to shrink between 0.3 and 0.6 mm in [18] and [26] respectively. The value indicated by our model is 4.5 mm, hence, considering the scaling up of all linear lengths by a factor 10, this is in line with the biological equivalent. This result is also in line with the mass selection by averaging values available in the literature references quoted. The backward integration uses the typical take-off velocity of a locust as initial condition. The initial angle of the femur-tibia joint sets at about 45° . This value is higher than the 15° found in the literature [18]. This outcome depends on how the dynamical system is set and corresponds to the angle at which the backward integration reaches a null angular rate for the parameters provided. Different values of the setting parameters would return a different angle. However, as these parameters have been chosen by mimicking the characteristics of the biological tissues, the

difference can be related to the simplifications introduced in the modelling.

Considering linear springs as energy storing devices in describing the biological mechanism is, of course, a simplifying assumption. In a locust, the whole leg presents a number of tissues with different rigidities. The outer cuticle of the tibia, for instance, presents an area that buckles under compression stress enhancing the tibia folding movement in the pre-launch phase [19,27]. The same area presents little or no strain under tension stress. This is a variable geometry that cannot be captured by the simple model presented. The same applies for the bending moments in the tibia and femur producing elastic bending, hence storing more energy and affecting the dynamics on release. Moreover, both the femur and the tibia present a variable cross section, which is responsible for a non-uniform distribution of the stresses, along their axes. This was also observed in [18], where these effects were deemed too difficult to capture quantitatively. The inclusion of these and other effects in the modelling and the analysis here presented is beyond the scope of this work.

No data have been found about the joint friction in the entire biological leg, but measurements were taken at the femur-tibia joint, and in particular about the friction in this. Bennet-Clark [18] estimated the energy loss in the femur-tibia joints to be not bigger than 20%. This is done considering the amount of energy accumulated in the pre-launch stage and comparing to the kinetic energy released in the launch stage. The analysis in [18] considers a number of assumptions and does not consider the femur-body and the tibia-foot joints. Because of the scarcity of data, it was decided not to consider energy losses in this study. We looked at the kinematics and dynamics produced by the joints, knowing that, an engineering design should take into account energy losses due to friction, flexibility in the elements here considered rigid and, eventually, compensate for these to meet the required performance.

Attention has been paid to the effects of scaling such a mechanism to sizes more typical of rovers and hopping mechanisms available in the literature. Several scaling techniques have been proposed as each scaling transfers some characteristics neglecting others. This makes scaling a compromise and the method used should be tuned on a case by case basis [28]. In this study two strategies were proposed, one keeping the density constant, the other, inspired by structural engineering, keeping the Young module value constant. For the case of two torsional springs, both scaling methods returned similar outcomes, reproducing the trend of the locust-size device. However, for the case of one torsional, one in-line spring, both scaling methods fail to reproduce the dynamics. As scaling factor increases, so the motion of such a mechanism get farther from the one exhibited at small scale. It can be concluded that the design, more faithfully representing the geometry of locust legs presents some practical problems when it comes to scaling. This suggest considering the design with two torsional springs when moving beyond this theoretical study, onto the realisation of a mechanical prototype. It is conceivable the difference in trend between the small scale and the large scale mechanisms can be reduced by tuning parameters such as the natural (non stretched) length of the linear spring or the attaching point along the femur, both finding no equivalent in the biological case, as previously discussed. However, verifying these conjecture and understanding how the design can be made unaffected by scaling would require an in-depth analysis which is beyond the scope of this work. This study aims to assess the feasibility of the scaling rather than optimising a design for its easiness in scaling. For this reason no further analyses are done about the properties and performance of the scaled system. In this framework, results such as the initial angle of the foot-tibia joint for the scaled, two torsional spring system should not surprise. The research presented in this paper is in this sense a comparative study aiming to prove a

concept rather than optimising a hopper design.

This work looked also at the range attainable in presence of lift or thrust acceleration that effectively reduce the gravitational acceleration. The case for constant thrust direction was included in this study. It can be part of a real scenario when the main body of the vehicle has to keep a given attitude. This includes the realistic case of an hopper tasked to survey the ground during the aerial stages with an instrument mounted at a fixed angle with respect to the body. In this case, excluding independent thrust vectoring, the thrust direction remains constant in time. The analysis of this scenario highlights as, an increasing value of the thrust magnitude produces, intuitively, longer flights. The optimal launch angle is, in general, a function of the thrust direction. For arbitrary given magnitude and direction of the thrust, the inclination of the velocity vector at the lift-off to maximise the range is a nonlinear function of these two values. When just the thrust magnitude is assigned, the optimal launch angle and thrust direction angle can be chosen as function of the thrust magnitude only through Eq. (20). This ensures the maximisation of the range and provides a valuable tool in the design of a hopper to set the angle of the thruster with respect to the vehicle main body.

The option of using thrusters, as opposed to gliding devices, can be seen in a framework of space operations. It widens the possible operative scenarios reducing the risks linked to the unknown aerodynamic behaviour in extra-terrestrial atmosphere. Furthermore it allows for operations in vacuum (eg. asteroids or Moon surface). Finally, this propulsion choice appears to be popular in the literature about hopper for space exploration, especially in conjunction with the exploitation of in-situ resources [2, 4, 12–14]. The choice of not including the analysis of a landing stage is made as an analysis of the same depth as done with the launch stage would extend the scope of the work beyond reason. First the

attitude of the mechanism at the touch-down should be discussed, that would imply renouncing to the point mass model used in the aerial stage. The landing model should also include the terrain characteristics and an impact analysis featuring the identification of the first point of contact. In the authors' opinion this is achievable, and will probably be achieved in future works, after having refined the aerial stage and the attitude control of the mechanism during this.

8 Conclusions

This work presented a study on the design of a hopper where legs are inspired by the physiology of locusts and a propulsion system is proposed for the aerial stage. In this, it differs from the popular choice of considering gliding devices. The model proposed emulates to a good degree relevant characteristics of the locusts jumps. The proof of concept is obtained through a dry, yet efficient simplification aimed to substitute actuators with preloaded springs to produce the hop. Reproducing data referred to the mechanics of locust jump in the literature by scaling the system physical parameters, proves the value of this study.

The model presented can be used to map the hop range to the initial setting of the spring-based momentum-providing mechanism, and, more in general, defining the design of hoppers coupling the impulsive hop with continuous, constant thrust during the flight. The flight stage is analysed in as a range optimisation problem and an analytic expression is derived for the launch angle as function of the thrust characteristics. It is found that, for constant thrust, the optimal launch angle coincides with the thrust angle.

The scaling up, towards sizes of interest for mechanical realisation, highlights the limits of a too faithful mimicking of locust physiology, providing useful design directions in this sense.

This work inserts and in part bridges the gap between hoppers producing long range, powered hops and those relying on legs for short, subsequent jumps.

References

- [1] J. Young, S. M. Walker, R. J. Bomphrey, G. K. Taylor, and A. L. R. Thomas. Details of insect wing design and deformation enhance aerodynamic function and flight efficiency. *Science*, 325(5947):1549–1552, 2009.
- [2] D-R Yu, X-W Lv, W. Bao, and Z-L Yao. Preliminary design analysis of a hopper vehicle for Mars mission. *Proceedings of the Institution of Mechanical Engineers, Part G: Journal of Aerospace Engineering*, 224:283–291, 2010.
- [3] E. Shafirovich, M. Salomon, and I. Gokalp. Mars hopper versus mars rover. In *European Space Agency, (Special Publication) ESA SP*, number 542, pages 97 – 102, Noordwijk, Netherlands, 2003.
- [4] G. A. Landis, S. J. Oleson, and M. McGuire. Design study for a mars geyser hopper. In *50th AIAA Aerospace Sciences Meeting Including the New Horizons Forum and Aerospace Exposition*, Nashville, TN, United states, 2012.
- [5] P. Fiorini, S. Hayati, M. Heverly, and J. Gensler. A hopping robot for planetary exploration. In *Aerospace Conference, 1999. Proceedings. 1999 IEEE*, volume 2, pages 153–158 vol.2, 1999.
- [6] J. Burdick and P. Fiorini. Minimalist jumping robots for celestial exploration. *The International Journal of Robotics Research*, 22(7-8):653–674, 2003.

- [7] S. Ulamec, V. Kucherenko, J. Biele, A. Bogatchev, A. Makurin, and S. Matrossov. Hopper concepts for small body landers. *Advances in Space Research*, 47(3):428 – 439, 2011.
- [8] A. Dzaba, E. Mucasey, A. Abraham, T. Hart, and E. Schuster. State-feedback control of the spacehawk earth-based lunar hopper. In *Unmanned Aircraft Systems (ICUAS), 2013 International Conference on*, pages 628–633, May 2013.
- [9] B. Brown and G. Zeglin. The bow leg hopping robot. In *Robotics and Automation, 1998. Proceedings. 1998 IEEE International Conference on*, volume 1, pages 781–786 vol.1, May 1998.
- [10] T. Wu, T. J. Yeh, and B. Hsu. Trajectory planning of a one-legged robot performing a stable hop. *Int. J. Rob. Res.*, 30(8):1072–1091, July 2011.
- [11] M. Kovac, M. Schlegel, J. Zufferey, and D. Floreano. Steerable miniature jumping robot. *Autonomous Robots*, 28(3):295–306, 2010.
- [12] H. R. Williams, R.M. Ambrosi, and N. P. Bannister. A mars hopping vehicle propelled by a radioisotope thermal rocket: thermofluid design and materials selection. *Proceedings of the Royal Society A: Mathematical, Physical and Engineering Science*, 467(2129):1290–1309, 2011.
- [13] S. D. Howe, R. C. O’Brien, R. M. Ambrosi, B. Gross, J. Katalenich, L. Sailer, J. Webb, M. McKay, J. C. Bridges, and N. P. Bannister. The mars hopper: An impulse-driven, long-range, long-lived mobile platform utilizing in situ martian resources. *Proceedings of the Institution of Mechanical Engineers, Part G: Journal of Aerospace Engineering*, 225(2):144–153, 2011.
- [14] G. A. Landis and D. L. Linne. Mars rocket vehicle using in situ propellants. *Journal of Spacecraft and Rockets*, 38(5):730–735, 2001.

- [15] M. A. Woodward and M. Sitti. MultiMo-Bat: A biologically inspired integrated jumpinggliding robot. *The International Journal of Robotics Research*, 33(12):1511–1529, October 2014.
- [16] M. Kovac, W. Hraiz, O. Fauria, J.-C. Zufferey, and D. Floreano. The EPFL jumpglider: A hybrid jumping and gliding robot with rigid or folding wings. In *Robotics and Biomimetics (ROBIO), 2011 IEEE International Conference on*, pages 1503–1508, 2011.
- [17] A. L. Desbiens, M. T. Pope, D. L. Christensen, E. W. Hawkes, and M. R. Cutkosky. Design principles for efficient, repeated jumpgliding. *Bioinspiration & Biomimetics*, 9(2):12, 2014.
- [18] H. C. Bennet-Clark. The energetics of the jump of the locust *Schistocerca gregaria*. *The Journal of experimental biology*, 63(1):53–83, August 1975.
- [19] W. J. Heitler. The locust jump. *Journal of comparative physiology*, 89(1):93–104, 1974.
- [20] M. C. Birch, R. D. Quinn, G. Hahm, S. M. Phillips, B. Drennan, A. Fife, H. Verma, and R. D. Beer. Design of a cricket microrobot. In *Robotics and Automation, 2000. Proceedings. ICRA '00. IEEE International Conference on*, volume 2, pages 1109–1114 vol.2, 2000.
- [21] M. C. Birch, R. D. Quinn, G. Hahm, S. M. Phillips, B. Drennan, R. D. Beer, Xinyu Yu, S. L. Garverick, S. Laksanacharoen, A. J. Pollack, and Roy E. Ritzmann. A miniature hybrid robot propelled by legs. In *Intelligent Robots and Systems, 2001. Proceedings. 2001 IEEE/RSJ International Conference on*, volume 2, pages 845–851 vol.2, 2001.

- [22] V Zaitsev, O Gvirsman, U Ben Hanan, A Weiss, A Ayali, and G Kosa. Locust - inspired miniature jumping robot. In *International Conference on Intelligent Robots and Systems (IROS)*, Hamburg, Sept. 2015.
- [23] Dunwen Wei and Wenjie Ge. Research on one bio-inspired jumping locomotion robot for search and rescue. *International Journal of Advanced Robotic Systems*, 11(168), 2014.
- [24] Guoyu Zuo, Wentian Qu, and Daoxiong Gong. Posture optimization of the locust-like hopping robot during the take-off stage. In *34th Chinese Control Conference*, pages 6111–6115, Hangzhou, Jul 2015. IEEE.
- [25] G. Bonsignori, C. Stefanini, U. Scarfogliero, S. Mintchev, G. Benelli, and P. Dario. The green leafhopper, *Cicadella viridis* (Hemiptera, Auchenorrhyncha, Cicadellidae), jumps with near-constant acceleration. *The Journal of Experimental Biology*, 216(7):1270–1279, 2013.
- [26] M. Burrows and G. Morris. The kinematics and neural control of high-speed kicking movements in the locust. *Journal of Experimental Biology*, 204(20):3471–3481, 2001.
- [27] W. J. Heitler. The locust jump: Iii. structural specializations of the metathoracic tibiae. *The Journal of Experimental Biology*, 67(1):29–36, 1977.
- [28] Y. T. Cheng and C. M. Cheng. Scaling, dimensional analysis, and indentation measurements. *Materials Science and Engineering R: Reports*, 44:91–150, 2004.
- [29] G. Rastogi, K. Moin, and S. M. Abbas. Dimensional Analysis and Development of Similitude Rules for Dynamic Structural Models. *International*

Journal of Emerging Technology and Advanced Engineering, 5(3):68-72,
2015.

Appendix 1 Notation

a	length of the tibia extension where the in-line spring for the femur tibia joint is attached
b	distance along the femur from the femur-tibia joint at which the in-line spring for the femur tibia joint is attached
g	gravitational acceleration
k_1	in-line spring in the femur
k_2	in line or torsional spring for the femur-tibia joint
k_3	torsional spring in the tibia-foot joint
K_e	kinetic energy
l_3	half length of the tibia
m_1	mass of the body
m_2	mass of the femur
m_3	mass of the tibia and foot
N	scaling factor
t_f	flight time
T	acceleration produced by the thrust
V	potential energy
v_{des}	Desired take off velocity
v_L	take off velocity
x_1	horizontal coordinate of the body centre of mass
x_2	horizontal coordinate of the femur-tibia joint
x_3	horizontal coordinate of the tibia mid-point
y_1	vertical coordinate of the body centre of mass
y_2	vertical coordinate of the femur-tibia joint
y_3	vertical coordinate of the tibia mid-point

Continued on next page

Continued from previous page

Δ	distance between the femur-tibia joint and the body centre of mass
ξ	generic lagrangian coordinate
ψ	thrust angle with respect to the horizontal
Θ	launch angle with respect to the horizontal
θ_1	angle of the femur-tibia joint
θ_2	angle of the tibia-foot joint
\mathbb{Z}	set of all integer numbers (positive, negative or 0)

Subscripts

<i>comp</i>	identifies k_2 as a compression spring
<i>des</i>	desired value
<i>fin</i>	value at the end of the dynamic phase
<i>ini</i>	value at the beginning of the dynamic phase
<i>tors</i>	identifies k_2 as a torsional spring
0	value in static conditions
